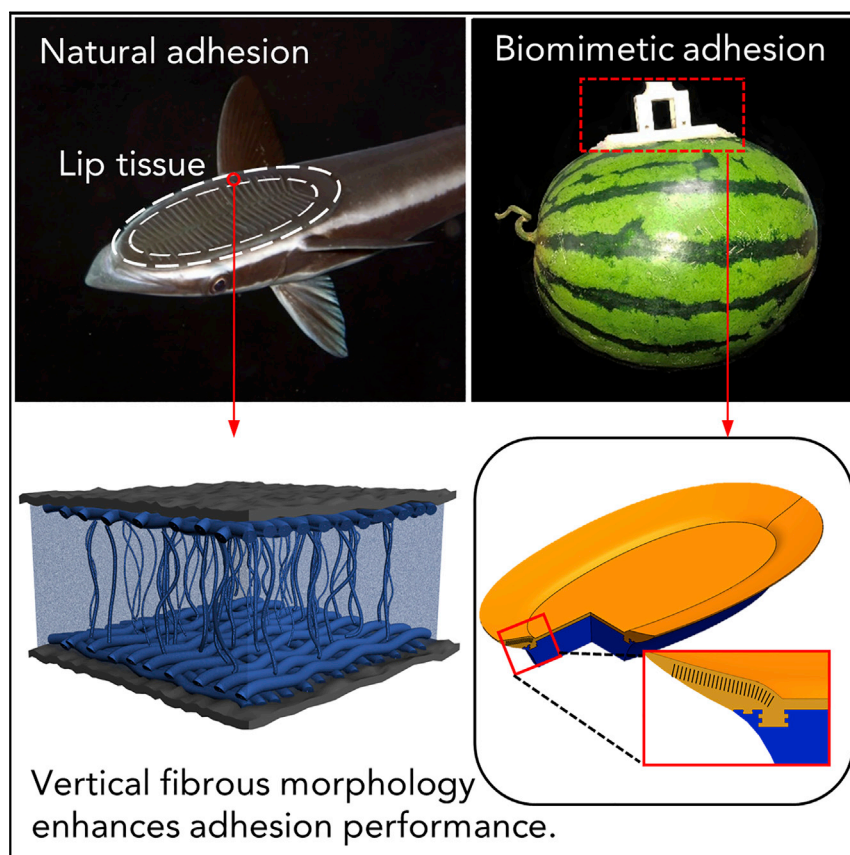


Article

Vertical Fibrous Morphology and Structure-Function Relationship in Natural and Biomimetic Suction-Based Adhesion Discs



The remora suckerfish uses multiple strategies in the suction disc to achieve robust adhesion. We demonstrate a unique strategy of vertical collagen fibrous structure in the soft disc lip tissue of remora. By creating a biomimetic prototype, such vertical fibrous morphology is validated to enhance adhesion performance substantially. The vertical fibrous morphology can also inspire novel designs of soft actuators with anisotropic properties.

Siwei Su, Siqi Wang, Lei Li, ..., Shaokai Wang, Juan Guan, Li Wen

juan.guan@buaa.edu.cn (J.G.)
liwen@buaa.edu.cn (L.W.)

HIGHLIGHTS

The lip tissue of remora's suction disc contains well-aligned collagen fibers

The structure in natural adhesion disc is remodeled as vertical fibers in matrix

Electrostatic flocking creates vertical nylon fiber morphology in silicone matrix

Vertical fibrous morphology is demonstrated to enhance soft adhesion and actuation



Understanding

Dependency and conditional studies on material behavior

Su et al., Matter 2, 1207–1221
May 6, 2020 © 2020 Elsevier Inc.
<https://doi.org/10.1016/j.matt.2020.01.018>



Article

Vertical Fibrous Morphology and Structure-Function Relationship in Natural and Biomimetic Suction-Based Adhesion Discs

Siwei Su,^{1,3} Siqi Wang,² Lei Li,² Zhixin Xie,² Fuchao Hao,¹ Jinliang Xu,⁵ Shaokai Wang,¹ Juan Guan,^{1,3,4,6,*} and Li Wen^{2,4,*}

SUMMARY

Recent years have seen rapid development in bio-inspired materials for adhesion. However, it remains challenging to realize robust adhesion on rough aquatic surfaces. An inspiring natural model is the remora fish, which has evolved to retain powerful adhesion to hosts using a dorsal suction disc. We find that the remora suction disc has a unique fibrous architecture of vertically oriented collagen fibers that enable anisotropic mechanical properties and enhanced adhesion performance. In the engineered prototype, vertically oriented nylon fibers are embedded into the soft silicone matrix using electrostatic flocking. The anisotropic mechanical properties are validated in both natural and biomimetic suction discs. Furthermore, the biomimetic suction disc demonstrates an enhanced adhesion function with a maximum 62.5% increase in pull-off force and a 340% increase in attachment time compared with the silicone control. This work can shed light on natural adhesion mechanisms and inspire novel designs for aquatic soft adhesives and actuators.

INTRODUCTION

Biological systems with high-performance adhesion abilities have attracted increasing interest to both elucidate the underlying mechanism of natural adhesion and inspire engineered adhesive devices.^{1–5} Recently, the remora suckerfish (*Echeneidae*) has attracted growing attention due to the unique underwater “hitchhiking” behavior that can form fast, reversible, and reliable attachment to the marine host, including sharks, sea turtles, and whales, using a distinct disc pad.^{5–9} During the attachment, remora can resist large forces generated by the host during swimming and leaping. The characteristic structure and parallel lamellae with aligned mineralized spinules increase the attachment force by creating high frictional forces between remora and the host.¹⁰ Simultaneously, the soft disc lip surrounding the lamellae also plays an important role by complying to the host surface and creating sufficient suction force (Figure 1A). However, in contrast to the number of studies conducted to understand the hard spinules and lamellae, thus far studies to reveal the internal structure of remora disc lip and its role in adhesion performance remain rare.

Soft biological sucker tissues are found in a variety of organisms and play important roles in the attachment due to the specially evolved internal structure and biomechanical properties. For example, octopus suckers consist of a three-dimensional (3D) fibrous network combining well-aligned muscle fibers that adjust the shape of the rim to create a seal, and randomly connected elastic fibers that store elastic energy and restore the shape of the sucker for extended attachment periods.^{11,12}

Progress and Potential

Soft yet robust adhesive structural materials are demanded for a variety of robotic applications in the aquatic environment. This work reveals the unique fibrous structure in the suction disc of the remora suckerfish, then designs and engineers a biomimetic prototype for suction-based adhesion. Fundamentally, the work proposes that the vertical fibrous structure enables anisotropic mechanical properties and enhanced adhesion performance in suction discs. Such a relationship is validated via the biomimetic prototypes with vertical nylon fibers embedded in a soft silicone matrix. The work offers new insights into the natural adhesion mechanisms and may revolutionize the design of suction-based adhesive devices for aquatic use.



Grasshopper, tree frog, sea urchin, and sea star also develop abilities to deform their attaching tissues viscoelastically to maximize contact with the substrate.¹³ The material basis for these attaching tissues is similar to that of other structural tissues such as ligaments and tendons, which have evolved to function for specific and periodic load-unload patterns. These tissues contain oriented collagen fibers ($E \sim 7\text{--}9$ GPa) to provide high stiffness for high load capacity, and elastin fibers ($E \sim 0.01\text{--}0.04$ GPa) to afford high elasticity.^{14,15} Revealing the design of materials inside remora disc lip and finding its role in the adhesion performance could elucidate the structure-property-function relationship of the remora's disc pad, which has not yet been reported. Moreover, investigations on mimicry of biological sucker tissue, especially the detailed internal structure, are still needed.

In the present work, we first described the unique fibrous architecture inside the remora disc lip. We then systematically evaluated the biomechanical properties of the natural disc lip and revealed its viscoelastic and anisotropic features. Using the electrostatic flocking technique, we designed and engineered a biomimetic lip composite with nylon fibers (diameter ~ 30 μm , length ~ 1.5 mm) of controllable orientations. The mechanical properties (tensile, compressive moduli, and creep resistance) of both natural tissue and biomimetic composite were then evaluated to validate the fibrous architecture-mechanical property relationship. Furthermore, the adhesion performance of suction discs from composite was evaluated. We finally demonstrated that the suction discs can attach to a wide variety of objects with different shapes and weights, and the anisotropic composite material could also enrich the designs of soft actuators. The work takes a step toward enhancing the suction performance of an artificial prototype by mimicking the fibrous structure and anisotropic mechanical properties of the remora sucker tissue. This study lays a foundation for bio-inspired soft adhesion devices and robust sealing materials, or even soft actuators for robotic applications.

RESULTS AND DISCUSSION

Morphology and Internal Structure of Remora Disc Lip

The surrounding, soft suction disc of remora is oval-shaped and the cross-section of the disc is wedge-shaped (Figure 1A). The histology images show clear characteristics of connective tissue (Figures 1C–1H), consisting of cells and an extracellular matrix (ECM) consisting of unique fibrous structure (Figure S1), whose main component is abundant, dense, coarse, and well-aligned collagen fibers, distributed in different layers. The Verhoeff Van Gieson (EVG) staining results also reveal that the ECM contains a little elastin (Figure S1A). The lip tissue is highly hydrated and the water content is estimated at around $84.4\% \pm 2.7\%$ by weighing the wet/dry mass.

According to the histology and scanning electron microscopy (SEM) images, the remora lip tissue can be modeled as three layers, corresponding to varied material morphology and mechanical role. The cross-sectional schematic view is illustrated in Figure 1B: (1) the outermost skin layer, (2) the under-skin layer, and (3) the central tissue section. The skin layer to directly contact the host appears rough on the surface and ~ 30 μm thin (Figure S1). The under-skin layer is $\sim 250\text{--}500$ μm thin, with layered horizontally compact collagen bundles ($\sim 40\text{--}60$ μm in diameter) (black arrows in Figures 1F–1H). In contrast, the central tissue section shows a distinctive cross-sectional morphology with vertically arranged and crimped/relaxed collagen fibers ($5\text{--}15$ μm in diameter and $300\text{--}550$ μm in length, indicated by red arrows in Figures 1F–1K). This central tissue constitutes up to $\sim 60\%$ of the thickness of the whole lip tissue. These central collagen fibers extend from both sides of the horizontal under-skin layer without a clear borderline, perpendicular to the inner and outer skin layer.

¹School of Materials Science and Engineering, Beihang University, Beijing 100191, China

²School of Mechanical Engineering and Automation, Beihang University, Beijing 100191, China

³International Research Center for Advanced Structural and Biomaterials, Beihang University, Beijing 100191, China

⁴Beijing Advanced Innovation Center for Biomedical Engineering, Beihang University, Beijing 100191, China

⁵School of Sino-French Engineer, Beihang University, Beijing 100191, China

⁶Lead Contact

*Correspondence: juan.guan@buaa.edu.cn (J.G.), liwen@buaa.edu.cn (L.W.)

<https://doi.org/10.1016/j.matt.2020.01.018>

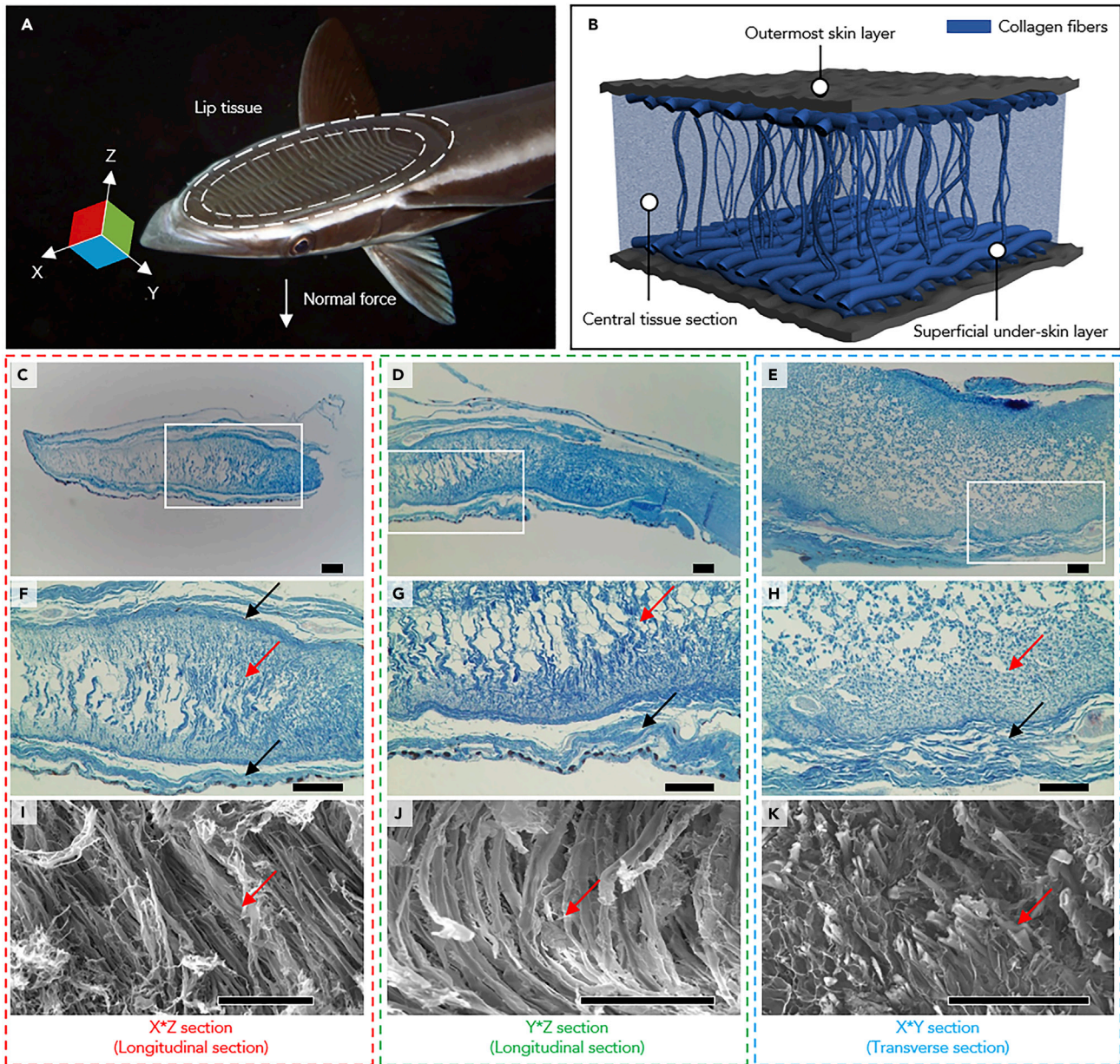


Figure 1. Structure and Morphology of the Remora Soft Suction Disc

(A) Dorsolateral view of remora fish highlighting the suction disc. Photo credit: Klaus M. Stiefel.
 (B) Schematic diagram of the three sections of the soft tissue in suction disc: outermost skin layer, superficial under-skin layer, and central tissue section. Collagen fibers are marked by bold curved lines in the central tissue section and under-skin layer.
 (C–H) Histology images of the cross-sections of remora soft disc tissue: x^*z section in (C) and (F), y^*z section in (D) and (G), and x^*y section in (E) and (H).
 (I–K) SEM images of the central tissue section of remora soft disc tissue: x^*z section in (I), y^*z section in (J), and x^*y section in (K).
 Red arrows indicate vertical crimped collagen fibers and black arrows indicate horizontal collagen fibers. All scale bars represent 200 μm .

It is noteworthy that the characteristic geometry and structure of the internal tissue in the remora suction disc have been rarely reported. Among other adhesive tissues, the octopus sucker tissue is more like active muscles arranged in a complex 3D array (radial, meridional, and circular), providing skeletal-like support for adhesion.^{11,12} The toe pad of tree frog presents a different morphology of sparsely distributed collagen and elastic fibers in the dermis, but the orientation of fibers has not yet

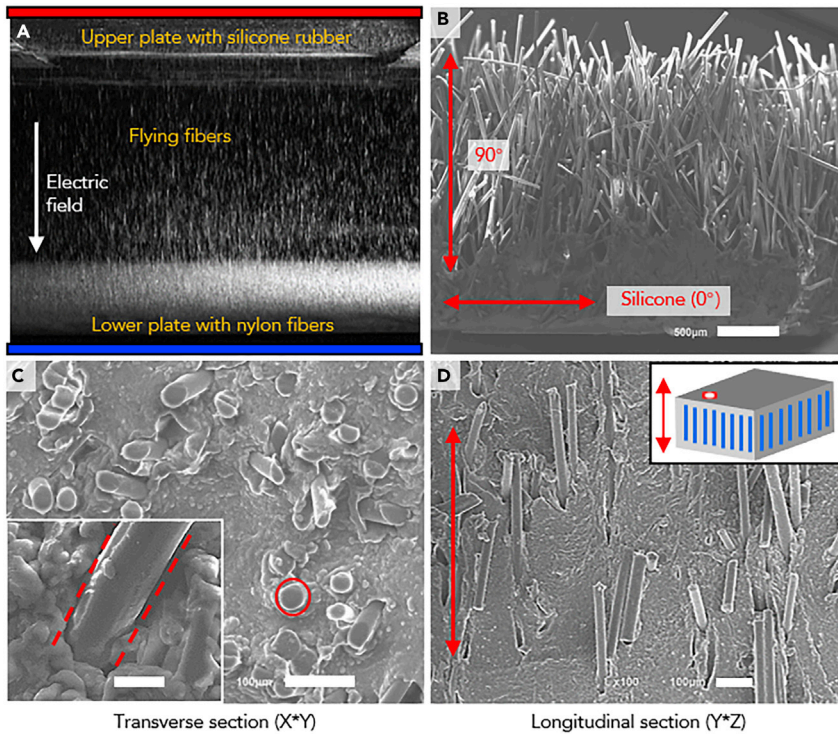


Figure 2. Fabrication and Morphology of Biomimetic Composite from Nylon Fiber and Silicone for the Suction Disc

(A) Principle of electrostatic flocking technique.

(B) Microscopic morphology of nylon fiber flocced silicone (side view). The vertical and horizontal arrows indicate the fiber orientation relative to the silicone substrate. Scale bar, 500 μm .

(C and D) Transverse section (C) and longitudinal section (D) of the nylon fiber/silicone composite. Circle and arrow indicate the fiber orientation. Scale bars, 100 μm . The inset in (C) highlights the well-adhered fiber-matrix interface (scale bar, 20 μm).

been characterized.^{16,17} It is proposed that the remora's unique tissue morphology of vertical fibers relative to the contact surface is important to the adhesion function, and we explore its structure-property-function relationship further through biomimetics and by engineering a synthetic prototype as follows.

Design and Fabrication of Biomimetic Remora Disc Lip Using Electrostatic Flocking

A number of strategies to mimic biological structures with controlled fiber alignment have been developed, including electrospinning,^{18,19} woven fabric,^{20,21} and 3D-printing techniques assisted by shear forces,²² electric fields,²³ and magnetic fields.^{24,25} However, we focus on mimicking the unique structure of remora disc lip with relatively large size (length ≥ 300 μm) and vertically oriented fibers inside a planar substrate. In this work, we applied electrostatic flocking^{26–28} to insert massive, short artificial fibers vertically onto a soft substrate to create a biomimetic tissue composite. The principle is electrostatic attraction and utilizing a controllable electric field to align conductive fibers vertically onto a receiving substrate (Figure 2A). Here we used nylon 66 fibers (elastic modulus $E \sim 2$ GPa, Figure S2), which are commonly used and widely available as reinforcement for soft matrices in composites.^{29,30} Vertical nylon fibers were placed onto a 500- μm -thick silicone layer (Ecoflex 0020, $E \sim 55$ kPa), and the morphology of the resultant nylon fibers flocced silicone is shown in Figure 2B, indicating that the vertically aligned fibers are well

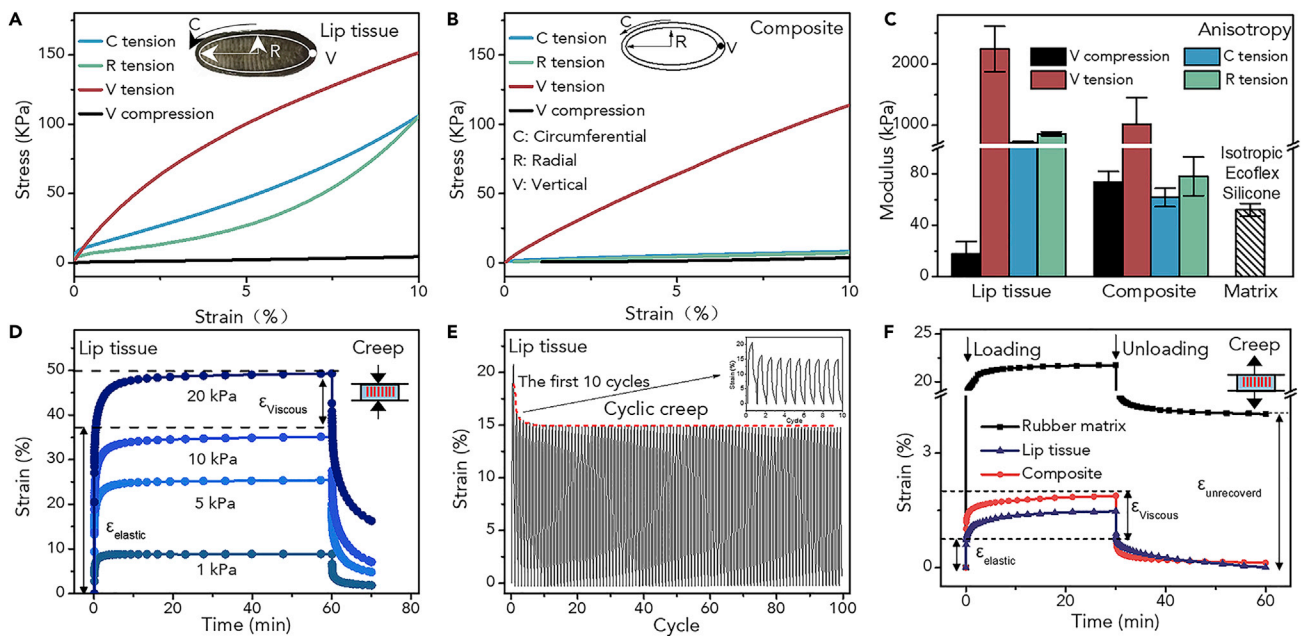


Figure 3. Mechanical Behavior and Properties of the Natural and Synthetic Suction Disc Materials

(A and B) Quasi-static stress-strain behaviors of natural disc tissue (A) and nylon fiber/silicone composite (B) in different directions demonstrating mechanical anisotropy.

(C) Moduli of lip tissues, nylon fiber/silicone composites in different directions, and pure silicone matrix ($n = 5$). Error bars denote \pm SD.

(D) Vertical compressive creep behaviors of natural lip tissue under stress of 1, 5, 10, and 20 kPa.

(E) Cyclic vertical compressive creep curve of lip tissue with 10 kPa stress loading for 6 s and stress releasing for 6 s.

(F) Vertical tensile creep behaviors of rubber matrix (Ecoflex), natural tissue, and composite under stress of 10 kPa.

fixed into the silicone substrate. In our experiment, the flocking density can reach ~ 120 fibers/ mm^2 (about 8% estimated from cross-sectional area analysis) in seconds under 500 kV/m electric field. The electrostatic flocking equipment and the process of the electrostatic flocking can be seen in [Figure S3](#) and [Video S1](#), respectively.

The nylon fiber flocked silicone was then embedded into a 3D-printed mold, which was filled with uncured silicone elastomer. The curing reactions that release heat and reduce the volume of the composite also enhance the fiber-matrix interfacial contact. A biomimetic disc prototype was eventually successfully fabricated, whose geometrical features were similar to that of the natural counterpart ([Figure S4](#); [Tables S1](#) and [S2](#)). The SEM images of the cross-sectional view show vertically standing fibers ([Figures 2C](#) and [2D](#)) and the seamless contact between nylon fibers and silicone matrix in the biomimetic remora disc lip (inset image of [Figure 2C](#)).

Mechanical Properties of the Remora Disc Lip Tissue and the Biomimetic Composite

We firstly evaluated the quasi-static mechanical properties of both natural and biomimetic lip materials. Tension tests perpendicular to/along the fiber axis and compression tests along the fiber axis were conducted. The representative tensile stress-strain curves of natural remora disc lip tissue in three directions and the compressive stress-strain curve in the fiber axis (V direction) are plotted in [Figure 3A](#). The mechanical properties (modulus, breaking strain, and breaking stress) are summarized in [Table 1](#). The tensile stress-strain responses display non-linear and inelastic behaviors, and tensile responses along the circumferential and radial directions are very similar. The tensile moduli ([Figure 3C](#)) from the linear slope of 0%–5% strain are 725 ± 196 kPa, 864 ± 334 kPa,

Table 1. Mechanical Properties of Natural Remora Lip Tissue and the Composite

	Circumferential Tension			Radial Tension			Vertical Tension	Vertical Compression
	Modulus (kPa)	Breaking Stress (kPa)	Breaking Strain (%)	Modulus (kPa)	Breaking Stress (kPa)	Breaking Strain (%)	Modulus (kPa)	Modulus (kPa)
Natural tissue	725 ± 197	2175 ± 555	80 ± 12	864 ± 334	1734 ± 769	65 ± 9	2248 ± 371	17.7 ± 9.7
Composite	62 ± 7	/	/	78 ± 15	/	/	1013 ± 435	74 ± 8

and 2248 ± 371 kPa in circumferential, radial, and vertical directions, respectively, indicating distinctive mechanical anisotropy perpendicular to/along the fiber axis. When large extension $>10\%$ is reached, the curves in circumferential and radial directions experience obvious uplift in stress, indicating strain-hardening. In contrast, the compressive modulus in the vertical direction is much smaller (17.7 ± 9.7 kPa). Therefore, the vertical tensile modulus of natural remora lip tissue is 2- to 5-fold greater than the circumferential and radial modulus and two orders of magnitude greater than the vertical compressive modulus. Compared with the moduli of natural soft tissues reported previously, the radial and circumferential tensile modulus of remora disc lip tissue is comparable with the fish skin and muscle tissue,³¹ whereas the vertical compressive modulus is comparable with that of other sucker tissues, such as toe pad of tree frogs ($E \sim 4\text{--}25$ kPa),³² octopus sucker ($E \sim 10$ kPa),³³ grasshopper ($E \sim 20\text{--}65$ kPa),³⁴ and tube feet discs of sea stars ($E \sim 6.0$ kPa) and sea urchins ($E \sim 8.1$ kPa).³⁵

Clearly, the mechanical characteristics of remora lip tissue are a result of the distinctive fibrous architecture and structural anisotropy. The vertically standing collagen fibers in the central section lead to high vertical tensile modulus and low compressive modulus due to buckling and crimping, and the woven collagen fibers in the under-skin layer can resist tensile deformation and lead to a comparable tensile modulus on the circumferential and radial direction. In addition, the strain-hardening behavior in circumferential and radial directions may be explained by the crimped skin layers. [Figure S1A](#) provides a measurement of the wavy and straightened lengths of the superficial under-skin layer, corresponding well to the start of strain hardening (from $\sim 15\%$ to 35%). When fibers are straightened, the tension changes from stretching out the fiber waves to directly stretching the fibers, indicating significant stiffening. The cyclical creep curve of lip tissue in circumferential tension under 200 kPa also proved the strain-hardening effect ([Figure S5](#)).

For the biomimetic tissue composite, the quasi-static mechanical properties of the vertical nylon-fiber-reinforced silicone were also characterized in three directions under tensile/compression ([Figure 3B](#)). The tensile modulus ([Table 1](#) and [Figure 3C](#)) of the synthetic composite are 62 ± 7 kPa, 78 ± 15 kPa, and $1,013 \pm 435$ kPa in circumferential, radial, and vertical directions, respectively. The vertical tension modulus of the synthetic composite is 10- to 20-fold higher than the circumferential and radial modulus, as well as the vertical compression modulus (74 ± 8 kPa). Mechanical anisotropy is clearly realized in the synthetic counterpart. Compared with isotropic pure matrix (Ecoflex silicone, $E \sim 55$ kPa), the biomimetic composite with aligned nylon fibers mimics the vertical fibrous morphology of the natural remora disc lip tissue and emulates the anisotropic mechanical characteristics. The finite element modeling (FEM) results also show the contribution of fibers to increasing vertical tensile modulus and limiting tensile deformation, as the value of $\sigma_{\text{Von-Mises}}$ (equivalent stress) on fibers was higher than that of silicone matrix ([Figure S6](#)).

Natural tissues and biomimetic synthetics made from polymers commonly feature viscoelasticity and time-dependent mechanical behavior. Thus, we also performed

loading/unloading cyclical tests, creep tests, and dynamic tests of varying frequencies to reveal the materials' structure and property change as a function of time/frequency. [Figure 3D](#) displays the creep curves of the natural lip tissue under 1, 5, 10, and 20 kPa compressive stress in the vertical direction. Lip tissues were subject to a 60-min loading followed by a 10-min recovery. After applying the stress, the lip tissue immediately recovers with a sharp elastic strain, and the viscous strain gradually develops in ~ 10 min until reaching a plateau strain. As the creep stress increases, the characteristic time to reach the plateau strain increases. The slope for the strain/stress trendline also decreases ([Figure S7](#)), indicating a stiffening effect under increased compressive stress.

The cyclical vertical compressive creep behavior is shown in [Figure 3E](#). Throughout the repetitive (100 times) compressive loadings-unloadings (10 kPa), the creep strain of each cycle is consistent and stable. This means the natural tissue can sustain periodic loadings at stress levels of 10 kPa and behave reliably to ensure numerous episodes of adhesion during remora's lifetime.

In addition, the mechanical properties of natural remora disc lip tissue are frequency dependent, as shown in [Figure S8A](#). As the compression frequency increases, both storage modulus E' and loss modulus E'' increase. E' increases from 20 to 90 kPa and E'' increases from 10 to 25 kPa for two decades of frequency increase. Furthermore, the loading-unloading curve ([Figure S8B](#)) shows an apparent hysteresis loop, indicating that the natural lip tissue can dissipate up to $\sim 70\%$ energy at a compressive stress of 5 kPa.

The tensile creep behaviors of natural lip tissue, pure rubber matrix, and composite were examined for a 30-min creep under 10 kPa tensile stress and 30 min of recovery ([Figure 3F](#)). After applying the tensile stress, the rubber matrix, natural tissue, and the composite displayed a sharp elastic strain $\epsilon_{\text{elastic}}$ and a slow viscous $\epsilon_{\text{viscous}}$ as a function of time. After unloading, the elastic strain instantly recovered and the viscous strain slowly decreased. The fast equilibrium of creep strain helps to resist the deformation under the drag of the host, which was specifically reflected in less overall strain, less viscous strain, and less unrecovered strain. We applied the Burgers model to analyze the tensile creep behavior ([STAR Methods](#)). The experimental creep data in [Figure 3F](#) were fitted with the Burgers model with $R^2 > 0.96$, and the four parameters are summarized in [Table S3](#). The fitting results indicate that the composite had elastic modulus $E_1 = 891$ kPa, which is ~ 10 -fold that of pure silicone rubber. This is consistent with the quasi-static tensile test results. The retardation time τ for the viscoelastic element followed the order $\tau(\text{composite}) < \tau(\text{natural tissue}) < \tau(\text{rubber})$. In general, the greater elastic moduli, shorter retardation time, and lower viscosity of the biomimetic lip composite could lead to a more solid-like creep behavior, which could benefit the hitchhiking of remora, e.g., by helping to maintain the internal negative pressure and, thus, the adhesive force.

Adhesion Performance of the Biomimetic Suction Disc

The biomimetic composite combines the mechanical anisotropy and the viscoelastic behavior, which is hypothesized to bring forth improved adhesion performance. Here, two typical isotropic silicones for making suction discs are chosen as controls, the pure soft matrix rubber (Ecoflex silicone, $E \sim 55$ kPa) and another rubber (Mold-Star silicone, $E \sim 662$ kPa). The pull-off experiments ([Figure S9](#)) are conducted under different applied preload forces (1, 5, 10, 15, and 20 N) underwater, and representative change of normal force during the attachment and detachment is shown in [Figure 4A](#). Smooth and rough ($R_a = 200$ μm) surfaces were chosen as substrates.

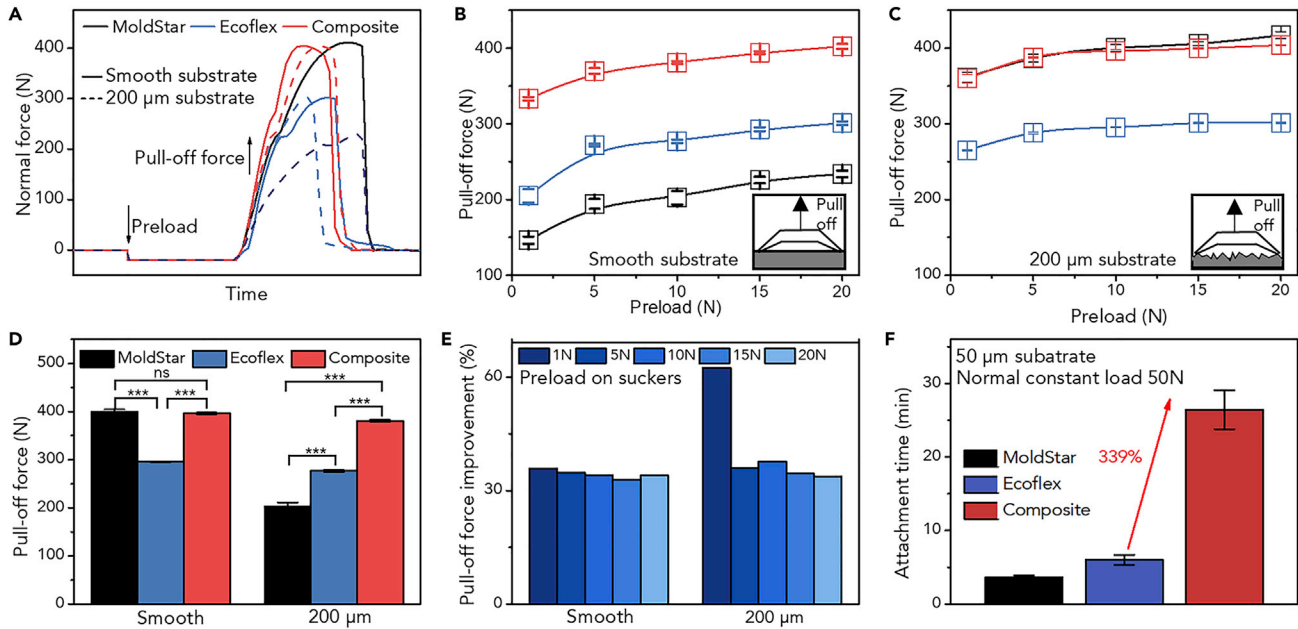


Figure 4. Underwater Attachment Performance of the Biomimetic Suction Discs

(A) Representative force-time profiles of the synthetic discs made from Ecoflex, MoldStar, and nylon fiber/silicone composite with a preload of 20 N on smooth and rough ($R_a = 200 \mu\text{m}$) surfaces underwater.

(B and C) Pull-off force as a function of preload force (1, 5, 10, 15, and 20 N) on smooth (B) and rough (C) surfaces ($n = 5$). Error bars denote \pm SD.

(D) Pull-off force or maximum detachment force of the synthetic disc from (A). *** $p \leq 0.001$; ns, not significant. p values were determined by Student's t test.

(E) Adhesion enhancement of composite disc with 1–20 N preload on smooth and $R_a = 200 \mu\text{m}$ substrate compared with pure silicone disc.

(F) Attachment time of the suckers under a constant 50-N load on a $R_a = 50 \mu\text{m}$ substrate ($n = 5$). Error bars denote \pm SD.

When an external preload was exerted on the suction disc, the disc makes contact with the substrate to form a seal and the water inside the disc is discharged to cause a pressure difference. As shown in Figure S10, when the disc has a lower vertical compressive modulus, it can follow the contours of a substrate to form a better seal and maintain the pressure differential. During the detachment process, the disc internal volume and the pressure differential increase (Figure S11A). The edge of the disc deformed toward the center of the disc, caving inward, eventually causing the attachment to fail, and both the force and the pressure differential drop to zero. The fibrous structure embedded in the composite disc delays the process of caving inward, restrains the deformation caused by pull-off force while maintaining a good seal with the substrate, and eventually results in a significantly higher pressure differential and higher pull-off force (Figures 4B and 4C; Videos S2 and S3). The biomimetic composite disc generates a considerable pull-off force in the ambient underwater environment, measuring up to 404 N on the smooth surface and 402 N on the rough surface. Compared with the two pure silicone suction discs, the biomimetic composite disc shows greater pull-off force on both surfaces, whereas the soft silicone (Ecoflex) suction disc shows smaller pull-off force on both surfaces, with a non-significant difference in pull-off force between the two surfaces (302 N and 301 N on the smooth and rough surface, respectively). The pull-off force of the stiffer silicone (MoldStar) suction disc is reduced dramatically from smooth (417 N) to rough (234 N) surfaces. Ecoflex has a higher surface roughness than MoldStar (Figure S12), which is supposed to decrease attachment performance of a suction disc made of Ecoflex, but on the other hand the softer Ecoflex-based suction disc can deform more easily. The composite suction disc can maintain the highest pressure

differential, thus resulting in better pull-off performance (Figures 4D and S11B). We observe maximum adhesion enhancement of 62.5% using the fiber-reinforced adhesive disc on the rough surface ($R_a = 200 \mu\text{m}$) that is comparable with that of the adhesive disc made of pure Ecoflex silicone (Figure 4E). Moreover, a preload of 1 N is sufficient for the composite disc to achieve robust, high pull-off force ($\sim 333 \text{ N}$) even on the rough surface ($R_a = 200 \mu\text{m}$). The pull-off stress σ ($\sigma = F/A$, where A represents the area of the disc pad) can be calculated. The biomimetic composite disc possesses σ ranging from 50 to 57 kPa on smooth surfaces to 47 to 57 kPa on the $R_a = 200 \mu\text{m}$ rough surfaces both with 1–20 N preload, compared with 50 to 80 kPa for commercial suction cups on smooth surfaces. The suction pad of the biological remora could achieve a pull-off force of 79.0 N and stress of 46.6 kPa on sharkskin surface ($R_a \sim 120 \mu\text{m}$),³⁶ and our biomimetic sucker achieves a force value close to these biological data. In addition, the sucker can repeat at least 100 cycles without a significant decrease in the pull-off force (Figure S13).

During hitchhiking, remoras need to maintain attachment on a wide range of surfaces. Therefore, a sucker needs to be capable of maintaining robust and strong adhesion on rough surfaces under external load. Figure 4F shows the role of vertical fibers in maintaining the attachment on a rough ($R_a = 50 \mu\text{m}$) surface underwater. The underwater attachment time extended from $\sim 6 \text{ min}$ (pure silicone suction disc) to $\sim 26 \text{ min}$ (biomimetic composite suction disc), generating $\sim 340\%$ improvement, while the attachment time of the stiffer suction cup is only $\sim 4 \text{ min}$. The biomimetic sucker is also proved to improve the attachment time (generating a $\sim 270\%$ increase) on dry, smooth substrates (Figure S14). Concerning the suction on dry and rough substrates, the biomimetic suckers need to be connected to a vacuum pump to ensure initial sealing. Our results suggest that the biomimetic sucker is better at maintaining attachment due to the tensile creep resistance of the composite.

To verify the effect of fiber density in the composite, we have made composites with varied fiber densities and their corresponding suction discs. The results (Figure S15) show that higher fiber density results in higher vertical tensile modulus of the composite and higher pull-off forces of the suction disc on both smooth and rough ($R_a = 200 \mu\text{m}$) substrates underwater. However, limited by the equipment and fiber properties, the maximum fiber flocking density in this work is $\sim 8\%$.

For wider applications, we consider the fibrous structure embedded in materials as an effective strategy for improving pull-off force irrespective of the geometry of the suction disc. The vertically aligned fiber composite is incorporated into circular suction cups, providing over 50% pull-off force improvement (Figure S16). We also connect the fiber-reinforced sucker with tubing and a vacuum pump as a gripping system, which shows abilities to lift a wide range of objects with various sizes and shapes (Figure 5A). This fiber-reinforced sucker system possesses high surface conformability while simultaneously maintaining high pull-off force due to the deformability in radial and circumferential directions and high tensile vertical stiffness. While the fiber-reinforced sucker can easily lift the 280-g volleyball, the common silicone sucker cannot, thus demonstrating the superior suction adhesion performance of our fiber-reinforced composite sucker. Also, the biomimetic composite suction disc was used to suspend heavy and irregular objects such as a watermelon and 4 kg of bottled water in a moist environment to demonstrate the functionality (Figure 5B).

Adhesive systems based on mechanisms of mechanical interlocking, molecular attractions, and chemical-based gluing often lapse in an underwater

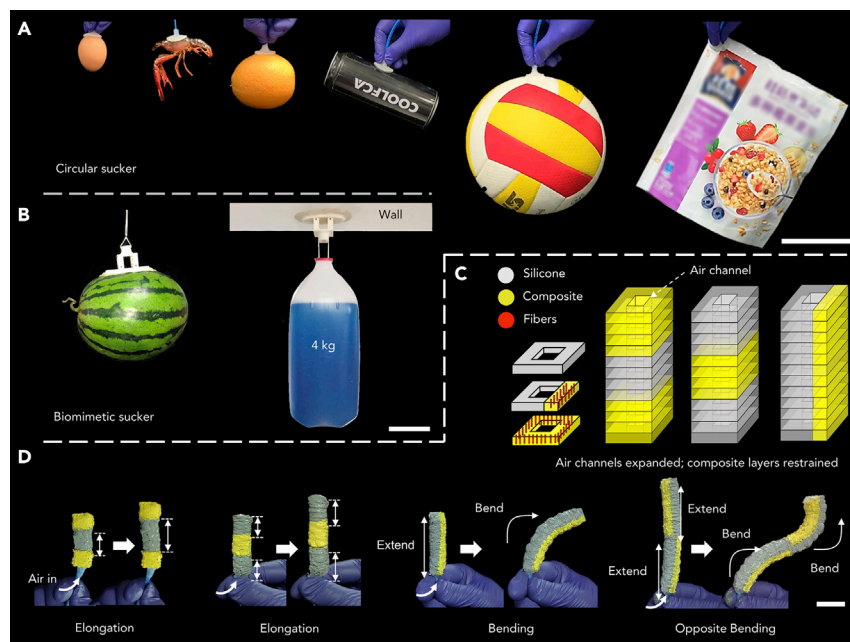


Figure 5. Demonstration of the Circular Suction Disc, Biomimetic Sucker, and Actuators

(A) Fiber-reinforced circular suction disc as gripper lifting various objects such as 75-g raw egg, 76-g alive crayfish, 216-g orange, 130-g bottle, 280-g volleyball, and 153-g plastic bag. Scale bar, 10 cm.

(B) Biomimetic sucker lifted a 5.5-kg watermelon and was attached to the wall with a load of 4 kg of water in a moist environment. Scale bar, 10 cm.

(C) Schematic diagrams of rubber block, anisotropic composite blocks, and structures of actuators.

(D) In these demonstrations, the inside vertical fibers limit the extension of the rubber matrix and result in special elongation and bending. Scale bar, 20 mm.

environment.^{1,37,38} By contrast, suction-based adhesive systems show robust, reversible, and repeatable adhesion under the wet conditions without causing chemical contamination, especially when connecting to a pump to allow internal pressure regulation.^{39,40} Furthermore, aquatic species, such as octopus,^{11,12} clingfishes,⁴¹ and leeches⁴² often rely on suction to achieve adhesion. In our work, we further improve the suction-based adhesion performance by putting vertically aligned fibers inside the composite sucker, which is inspired by remora.

Remoras use their suction pads to hitchhike on marine hosts, thus to travel a long distance with minimal energy consumption. Other anisotropic adhesion pads in nature, such as octopus sucker, have a complex anisotropic muscular structure that can actively deform to capture prey or crawl on different surfaces.^{11,12} Terrestrial organisms, such as geckos, use their adhesion pad to obtain anisotropic adhesion when climbing on walls.⁴ However, the adhesion mechanisms (van der Waals forces and capillary forces) that evolved in the terrestrial environment are of limited utility in underwater environments.

More interestingly, such strategies of fabricating composite materials with defined fiber orientation for morphology anisotropy can be applied in soft pneumatic actuators, i.e., for controlled deformation and “smart” behaviors. Because the fibers will limit the axial tensile deformation, by placing the fibers in the middle or at both ends, the soft pneumatic actuator can be elongated at a specific position without fiber; bending and asymmetric bending can be achieved by placing the fibers on one side or on different sides (Figures 5C and 5D). The quantitative data and process



are shown in [Figure S17](#) and [Video S4](#). These motions in actuators may enrich the locomotion of future soft robotics across scales.

Conclusions

In the present work, the natural soft suction disc of the remora fish is shown to consist of a 3D fibrous network and vertical collagen fibers in the central section. Such vertical fibrous architecture demonstrates a high tensile modulus and a low compressive modulus. We hypothesized that remora suckerfish evolved this feature for the adhesion function.

In the biomimetic prototype of the suction disc, a silicone-matrix composite with vertically aligned nylon fibers using the electrostatic flocking technique is employed. The electrostatic flocking technique demonstrates a low-cost and straightforward technique to prepare anisotropic fibrous morphology in composites. The biomimetic composite, with $\sim 1,000$ kPa vertical tensile modulus and ~ 70 kPa compressive modulus, generates both anisotropic morphology and anisotropic mechanical properties comparable with those of natural tissue. Compared with pure silicone disc, the fibrous composite endows the biomimetic disc with significantly longer attachment duration ($\sim 340\%$) and demonstrates an enhanced pull-off force ($>50\%$) for the circular suction cups. Overall, the soft silicone matrix in the composite ensures sufficient contact irrespective of the substrate surface roughness, whereas the vertically standing fiber in the composite ensures robust attachment and resists creep under challenging conditions.

In the future, the inclusion of woven fibrous layers to mimic the skin layers of the natural suction disc would be expected to further complement the synthetic model. More tissue-like materials could be implemented, thus to better mimic the natural tissues' mechanical properties. As for electrostatic flocking technology, there are also limitations in controlling the alignment of the fibers and the fiber density. New technologies and materials are still needed to improve the orientation of millimeter-long fibers and the fiber flocking density. Besides, we did not find a clear mathematical model to correlate materials' mechanical properties with the suction-based adhesion function. Theoretical research will greatly facilitate the selection of materials and the optimization of adhesion systems. Furthermore, combining the biomimetic fibrous structure with the concepts of coiled and stimuli-responsive fibers may potentially improve the performance of fiber-reinforced suckers and actuators.⁴³ Such work can deepen our understanding of structure-property-function relationships in biological suction systems, and lead to novel designs and fabrication routes for improved adhesion performance in soft robotics.

EXPERIMENTAL PROCEDURES

Characterization of the Morphology and Microstructure

For SEM images, biological lip tissue samples were quickly frozen with liquid nitrogen and transferred to a freeze-dryer (Alpha 1-2 LD plus; Martin Christ Gefriertrocknungsanlage, Germany). The temperature was -50°C with a vacuum pressure of 0.12 mbar over 24 h. Blocks were cut out in three sections along vertical, circumferential, and radial directions. The cross-sections were then sputter-coated with palladium for 120 s and images were taken on a scanning electron microscope (JSM 6010; JEOL, Tokyo, Japan). For the histological investigation, the lip tissues were fixed in 4% paraformaldehyde/phosphate-buffered saline (PBS) over 24 h and were then paraffin-embedded, sectioned, and stained for Masson's trichrome, which stains collagen blue and muscle fibers red. Tissue sections were scanned using an optical microscope (XSP-12CA; Shanghai Optical Instrument Factory, Shanghai, China). For the biomimetic sucker prototype, the blocks were cut off as described earlier

with the same initial sample preparation procedures (without freeze-drying) as for SEM.

Biomimetic Sucker Design and Fabrication

The dimensional parameters of the remora suction disc were measured to facilitate the biomimetic suction design (Tables S1 and S2). The suction disc prototype and mold for casting were designed using 3D computer-aided design software (SolidWorks, 2016). The mold was 3D-printed using photosensitive resin UTR9000. For fabrication of the biomimetic sucker, uncured Ecoflex was firstly coated with a thickness of $\sim 500\ \mu\text{m}$ on a polyethylene terephthalate film using a blade coater (Elcometer 4340; Elcometer Instruments, Manchester, UK), preventing fibers penetrating through the matrix during electrostatic flocking. Custom-built electrostatic flocking equipment consisting of electrodes ($400 \times 400 \times 5\ \text{mm}$), a power supply (up to 100 kV), and an insulation shell was employed. Thin semi-cured Ecoflex as an adhesive layer to fix the nylon fibers was coated on $\sim 500\text{-}\mu\text{m}$ Ecoflex film. The maximum flocking density was achieved in seconds with a voltage of $\sim 50\ \text{kV}$, current of $50\ \mu\text{A}$, and electrode distance of 10 cm. Nylon fibers $\sim 30\ \mu\text{m}$ in diameter and $\sim 1.5\ \text{mm}$ in length were aligned vertically into the semi-cured Ecoflex. By placing a reduced amount of fibers on the lower electrode plate, varied fiber density was achieved. The nylon fiber flocked silicone was put in a mold with uncured Ecoflex at room temperature for a further cure for $\sim 4\ \text{h}$. The silicone lips were glued with the resin parts using adhesives (Sil-poxy; Smooth-on, Easton, PA, USA). For comparison with the biomimetic sucker, hard silicone (MoldStar 30; Smooth-on) was also used to fabricate a synthetic sucker (without fiber). The materials stiffness of the biomimetic sucker components is summarized in Table S4.

Characterization of Materials Mechanical Properties

A Dynamic Mechanical Analyzer (DMA Q800; TA Instruments-Waters, New Castle, DE, USA) was used to conduct mechanical tests on natural tissues, pure silicone, and composite materials. The testing specimens were dissected from the biological and biomimetic sucker according to testing requirements. In the quasi-static circumferential and radial tensile tests, cuboid specimens or blocks of $4.0 \times 2.0 \times 0.6\ \text{mm}$ were used. For quasi-static vertical tensile and compressive tests, columnar specimens ($\sim 3\ \text{mm}$ diameter, $\sim 1.5\ \text{mm}$ thickness) were used. Specimens from biological lip tissue were immersed in PBS for 2 h before testing. Vertical tensile modulus was measured by a specially designed device (Figure S18). Using a fast-drying adhesive, two sides of the columnar specimens were glued on a custom-built clamp (based on the geometry of the compression clamp). After rehydrating, the specimens were stretched to failure, which occurs in the adhesive layer. All measurements ($n = 5$ for each group) were performed with a ramping force of $0.6\ \text{N/min}$. The modulus was defined as the slope of the linear segment in the stress-strain curve. In the creep and cyclic creep tests, the geometry parameters of biological and biomimetic specimens were the same as in the quasi-static test. During all the tests for the biological samples, the space between the upper and lower clamp was filled with PBS solution to ensure the samples remained moist. For creep compressive tests, the biological samples underwent 60 min of loading and 10 min of recovery at four creep stresses of 1, 5, 10, and 20 kPa at room temperature. For cyclic creep compressive tests, the biological samples were tested for 6 s of loading of 10 kPa and 6 s of recovery, repeated 100 times. For creep tensile tests, the custom-built device for specimen fixation is shown in Figure S18. The pure silicone and biomimetic composite underwent 30 min of loading and 30 min of recovery at creep stress of 10 kPa at room temperature. For frequency sweep tests, the top clamp was lowered to contact the sample surface until a load of $1\ \mu\text{N}$ was achieved. Frequency sweeps

(0.1–10 Hz, 5 points per decade) were conducted at 1% strain. For loading-unloading tests, loading and unloading velocities were 50 kPa/min.

Pull-Off Force, Attachment Time, and Pressure Measurements

The pull-off forces (maximum adhesion force) and pressure were measured using custom-built adhesion testing equipment (Figure S9). The system consists of four main components: a materials testing machine (MTS model e44; MTS, Eden Prairie, MN, USA), a platform with substrates (smooth, $R_a = 50 \mu\text{m}$ and $R_a = 200 \mu\text{m}$), a water chamber, and a high-precision digital pressure switch (ZSE30AF/ISE30A; SMC, Tokyo, Japan). The suckers were fixed on the upper clamp and suction-adhered onto substrates with different preload forces (1, 5, 10, 15, and 20 N). The upper clamp was then moved upward at 10 mm/s until the suckers completely detached. We repeated all measurements at least five times in each condition. Results were summarized from five trials. The attachment time was measured on another mechanical testing machine (Zwick z0.5; Zwick/Roell, Ulm, Germany) with the same equipment as for pull-off forces testing. The suckers were attached with 15 N preload and moved upward with a tensile creep force of 50 N until detachment. The measurements were repeated at least five times in each case. Results were also averaged from five trials.

DATA AND CODE AVAILABILITY

The raw data associated with the figures and tables of this paper will be provided by the corresponding authors upon request.

SUPPLEMENTAL INFORMATION

Supplemental Information can be found online at <https://doi.org/10.1016/j.matt.2020.01.018>.

ACKNOWLEDGMENTS

This work was supported by the Fundamental Research Funds for the Central Universities, National Natural Science Foundation of China support projects, China (grant no. 91848105); and National Natural Science Foundation support projects 61822303, 61633004, and 91848206 in part by National Key R&D Program of China (grant nos. 18YFB1304600 and 2019YFB1309600).

AUTHOR CONTRIBUTIONS

S.S., S.W., J.G., and L.W. conceived the project. S.S. and J.G. conducted and characterized the morphology and mechanical properties of biological remora lip tissue and synthetic materials. S.S., L.L., F.H., and L.W. designed and fabricated the biomimetic remora discs. J.X. conducted the FEM simulations. S.S., S.W., L.L., and L.W. conducted attachment experiments. S.S., L.L., and L.W. conducted the demonstration of biomimetic suckers and actuators. S.S., J.G., and L.W. prepared the manuscript, and all authors provided feedback during subsequent revisions.

DECLARATION OF INTERESTS

The authors declare no competing interests.

Received: October 28, 2019

Revised: December 30, 2019

Accepted: January 23, 2020

Published: February 26, 2020

REFERENCES

- Baik, S., Kim, D.W., Park, Y., Lee, T., Bhang, S.H., and Pang, C. (2017). A wet-tolerant adhesive patch inspired by protuberances in suction cups of octopi. *Nature* 546, 396–400.
- Xue, L., Kovalev, A., Eichlerwolf, A., Steinhart, M., and Gorb, S.N. (2015). Humidity-enhanced wet adhesion on insect-inspired fibrillar adhesive pads. *Nat. Commun.* 6, 6621.
- Drotlef, D.M., Stepien, L., Kappl, M., Barnes, W.J.P., Butt, H.J., and Campo, A.D. (2013). Insights into the adhesive mechanisms of tree frogs using artificial mimics. *Adv. Funct. Mater.* 23, 1094.
- Tao, D., Xing, G., Lu, H., Liu, Z., Yong, L., Hao, T., Pesika, N., Meng, Y., and Yu, T. (2017). Controllable anisotropic dry adhesion in vacuum: gecko inspired wedged surface fabricated with ultraprecision diamond cutting. *Adv. Funct. Mater.* 27, 1606576.
- Wang, Y., Yang, X., Chen, Y., Wainwright, D.K., Kenaley, C.P., Gong, Z., Liu, Z., Liu, H., Guan, J., Wang, T., et al. (2017). A biorobotic adhesive disc for underwater hitchhiking inspired by the remora suckerfish. *Sci. Robot.* 2, eaan8072.
- Culler, M., and Nadler, J.H. (2014). Composite structural mechanics of dorsal lamella in remora fish. *MRS Proc.* 1619, <https://doi.org/10.1557/opl.2014.541>.
- Culler, M., Ledford, K.A., and Nadler, J.H. (2014). The role of topology and tissue mechanics in remora attachment. *MRS Proc.* 1648, <https://doi.org/10.1557/opl.2014.229>.
- Beckert, M., Flammang, B.E., and Nadler, J.H. (2016). A model of interfacial permeability for soft seals in marine-organism, suction-based adhesion. *MRS Adv.* 1, 2531–2543.
- Flammang, B.E., and Kenaley, C.P. (2017). Author correction: remora cranial vein morphology and its functional implications for attachment. *Sci. Rep.* 7, 5914.
- Beckert, M., Flammang, B.E., and Nadler, J.H. (2015). Remora fish suction pad attachment is enhanced by spinule friction. *J. Exp. Biol.* 218, 3551–3558.
- Kier, W.M., and Smith, A.M. (2002). The structure and adhesive mechanism of octopus suckers. *Integr. Comp. Biol.* 42, 1146–1153.
- Tramacere, F., Beccai, L., Kuba, M., Gozzi, A., Bifone, A., and Mazzolai, B. (2013). The morphology and adhesion mechanism of *Octopus vulgaris* suckers. *PLoS One* 8, e65074.
- Dodou, D., Breedveld, P., de Winter, J.C., Dankelman, J., and van Leeuwen, J.L. (2011). Mechanisms of temporary adhesion in benthic animals. *Biol. Rev. Camb. Philos. Soc.* 86, 15–32.
- Holzappel, G.A. (2001). Biomechanics of soft tissue. In *The Handbook of Materials Behavior Models*, J. Lemaitre, ed. (Academic Press), pp. 1049–1062.
- Meyers, M.A., Chen, P.Y., Lin, Y.M., and Seki, Y. (2008). Biological materials: structure and mechanical properties. *Prog. Mater. Sci.* 53, 1–206.
- Nakano, M., and Saino, T. (2016). Light and electron microscopic analyses of the high deformability of adhesive toe pads in White's tree frog, *Litoria caerulea*. *J. Morphol.* 277, 1509–1516.
- Drotlef, D.M., Appel, E., Peisker, H., Dening, K., Del, C.A., Gorb, S.N., and Barnes, W.J. (2015). Morphological studies of the toe pads of the rock frog, *Staurois parvus* (family: Ranidae) and their relevance to the development of new biomimetically inspired reversible adhesives. *Interface Focus* 5, 20140036.
- Courtney, T., Sacks, M.J., Guan, J., and Wagner, W.R. (2006). Design and analysis of tissue engineering scaffolds that mimic soft tissue mechanical anisotropy. *Biomaterials* 27, 3631–3638.
- Fisher, M.B., Henning, E.A., Söegaard, N., Esterhai, J.L., and Mauck, R.L. (2013). Organized nanofibrous scaffolds that mimic the macroscopic and microscopic architecture of the knee meniscus. *Acta Biomater.* 9, 4496–4504.
- Moutos, F.T., Freed, L.E., and Farshid, G. (2007). A biomimetic three-dimensional woven composite scaffold for functional tissue engineering of cartilage. *Nat. Mater.* 6, 162–167.
- Liao, I.C., Moutos, F.T., Estes, B.T., Zhao, X., and Guilak, F. (2013). Composite three-dimensional woven scaffolds with interpenetrating network hydrogels to create functional synthetic articular cartilage. *Adv. Funct. Mater.* 23, 5825.
- Compton, B.G., and Lewis, J.A. (2015). 3D-printing of lightweight cellular composites. *Adv. Mater.* 26, 5930–5935.
- Yang, Y., Chen, Z., Song, X., Zhang, Z., Zhang, J., Shung, K.K., Zhou, Q., and Chen, Y. (2017). Biomimetic anisotropic reinforcement architectures by electrically assisted nanocomposite 3D printing. *Adv. Mater.* 29, 1605750.
- Erb, R.M., Libanori, R., Rothfuchs, N., and Studart, A.R. (2012). Composites reinforced in three dimensions by using low magnetic fields. *Science* 335, 199–204.
- Martin, J.J., Fiore, B.E., and Erb, R.M. (2015). Designing bioinspired composite reinforcement architectures via 3D magnetic printing. *Nat. Commun.* 6, 8641.
- Uetani, K., Ata, S., Tomonoh, S., Yamada, T., Yumura, M., and Hata, K. (2015). Elastomeric thermal interface materials with high through-plane thermal conductivity from carbon fiber fillers vertically aligned by electrostatic flocking. *Adv. Mater.* 26, 5857–5862.
- Gossia, E., Tonndorf, R., Bernhardt, A., Kirsten, M., Hund, R.D., Aibibu, D., Cherif, C., and Gelinsky, M. (2016). Electrostatic flocking of chitosan fibres leads to highly porous, elastic and fully biodegradable anisotropic scaffolds. *Acta Biomater.* 44, 267–276.
- Takeshita, T., Yoshida, M., Takei, Y., Ouchi, A., Hinoki, A., Uchida, H., and Kobayashi, T. (2019). Relationship between contact pressure and motion artifacts in ECG measurement with electrostatic flocked electrodes fabricated on textile. *Sci. Rep.* 9, 5897.
- Devi, D.S.P., Bipinbal, P.K., Jabin, T., and Kutty, S.K.N. (2013). Enhanced electrical conductivity of polypyrrole/polypyrrole coated short nylon fiber/natural rubber composites prepared by in situ polymerization in latex. *Mater. Des.* 43, 337–347.
- Andideh, M., Naderi, G., Ghoreishy, M.H.R., and Soltani, S. (2014). Effects of nanoclay and short nylon fiber on morphology and mechanical properties of nanocomposites based on NR/SBR. *Fibers Polym.* 15, 814–822.
- Summers, A.P., and Long, J.H., Jr. (2005). Skin and bones, sinew and gristle: the mechanical behavior of fish skeletal tissues. *Fish Physiol.* 23, 141–177.
- Barnes, W.J.P., Goodwyn, P.J.P., Nokhbatolofoghahai, M., and Gorb, S.N. (2011). Elastic modulus of tree frog adhesive toe pads. *J. Comp. Physiol. A* 197, 969–978.
- Tramacere, F., Kovalev, A., Kleinteich, T., Gorb, S.N., and Mazzolai, B. (2014). Structure and mechanical properties of *Octopus vulgaris* suckers. *J. R. Soc. Interface* 11, 20130816.
- Jiao, Y., Gorb, S., and Scherge, M. (2000). Adhesion measured on the attachment pads of *Tettigonia viridissima* (Orthoptera, insecta). *J. Exp. Biol.* 203, 1887–1895.
- Romana, S., Stanislav, G., Valérie, J., and Patrick, F. (2005). Adhesion of echinoderm tube feet to rough surfaces. *J. Exp. Biol.* 208, 2555–2567.
- Beckert, M., Flammang, B.E., Anderson, E.J., and Nadler, J.H. (2016). Theoretical and computational fluid dynamics of an attached remora (*Echeneis naucrates*). *Zoology* 119, 430–438.
- Tinnemann, V., Hernandez, L., Fischer, S.C.L., Arzt, E., Bennewitz, R., and Hensel, R. (2019). In situ observation reveals local detachment mechanisms and suction effects in micropatterned adhesives. *Adv. Funct. Mater.* 29, 1807713.
- Kim, D.W., Baik, S., Min, H., Chun, S., Lee, H.J., Kim, K.H., Lee, J.Y., and Pang, C. (2019). Highly permeable skin patch with conductive hierarchical architectures inspired by amphibians and octopi for omnidirectionally enhanced wet adhesion. *Adv. Funct. Mater.* 29, 1807614.
- Silverman, H.G., and Roberto, F.F. (2007). Understanding marine mussel adhesion. *Mar. Biotechnol.* 9, 661–681.
- Kwak, M.K., Pang, C., Jeong, H.E., Kim, H.N., Yoon, H., Jung, H.S., and Suh, K.Y. (2011). Towards the next level of bioinspired dry adhesives: new designs and applications. *Adv. Funct. Mater.* 21, 3606–3616.

41. Ditsche, P., Wainwright, D.K., and Summers, A.P. (2014). Attachment to challenging substrates—fouling, roughness and limits of adhesion in the northern clingfish (*Gobiesox maeandricus*). *J. Exp. Biol.* 217, 2548–2554.
42. Kampowski, T., Eberhard, L., Gallenmüller, F., Speck, T., and Poppinga, S. (2016). Functional morphology of suction discs and attachment performance of the Mediterranean medicinal leech (*Hirudo verbana* Carena). *J. R. Soc. Interface* 13, 20160096.
43. Kanik, M., Orguc, S., Varnavides, G., Kim, J., Benavides, T., Gonzalez, D., Akintilo, T., Tasan, C.C., Chandrakasan, A.P., Fink, Y., et al. (2019). Strain-programmable fiber-based artificial muscle. *Science* 365, 145–150.

Matter, Volume 2

Supplemental Information

**Vertical Fibrous Morphology and Structure-
Function Relationship in Natural and
Biomimetic Suction-Based Adhesion Discs**

Siwei Su, Siqi Wang, Lei Li, Zhexin Xie, Fuchao Hao, Jinliang Xu, Shaokai Wang, Juan Guan, and Li Wen

Supplemental Figures

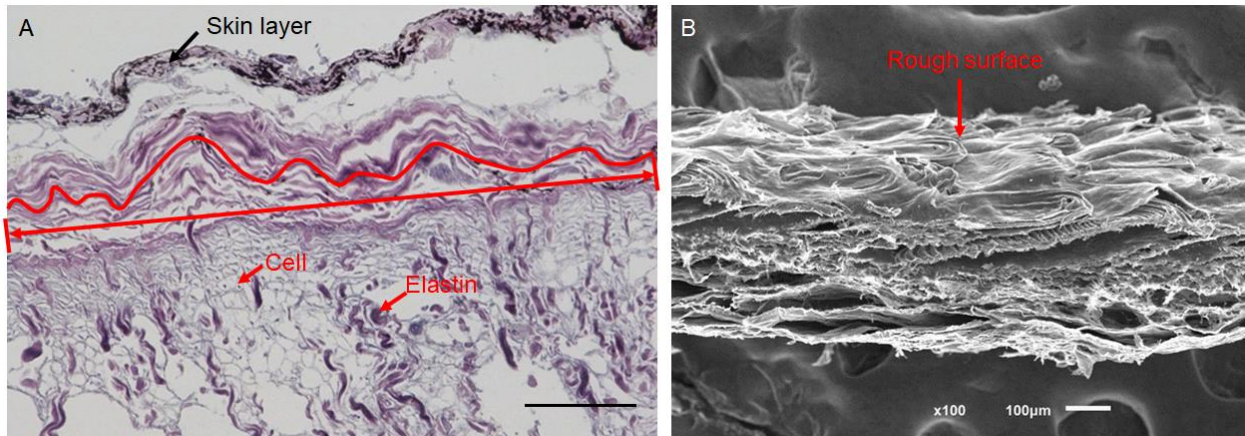


Figure S1. Morphology of lip tissue and the outmost skin. (A) EVG image of lip tissue in X*Z section, see legend of Figure 1. The EVG staining stains elastic fibers black and stains collagen fibers red. (B) Side-view of the skin peeled from the remora lip tissue. Scale bars, 100 μm .

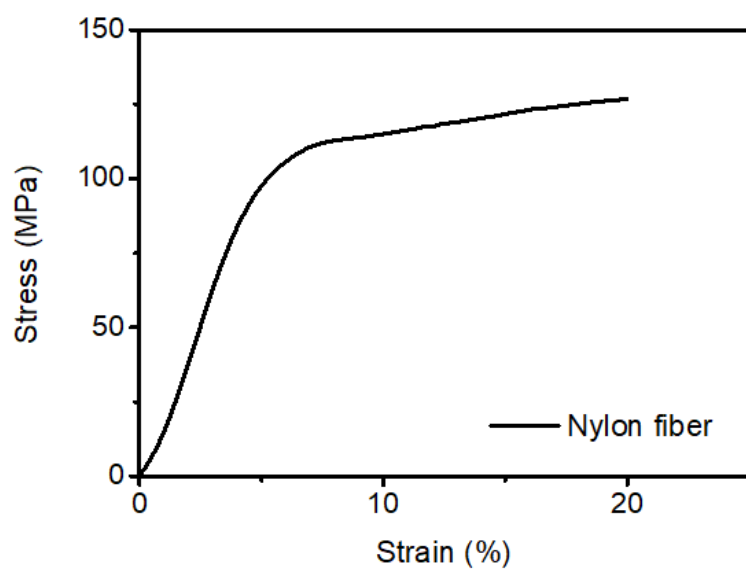


Figure S2. Stress-strain curve of nylon fiber.

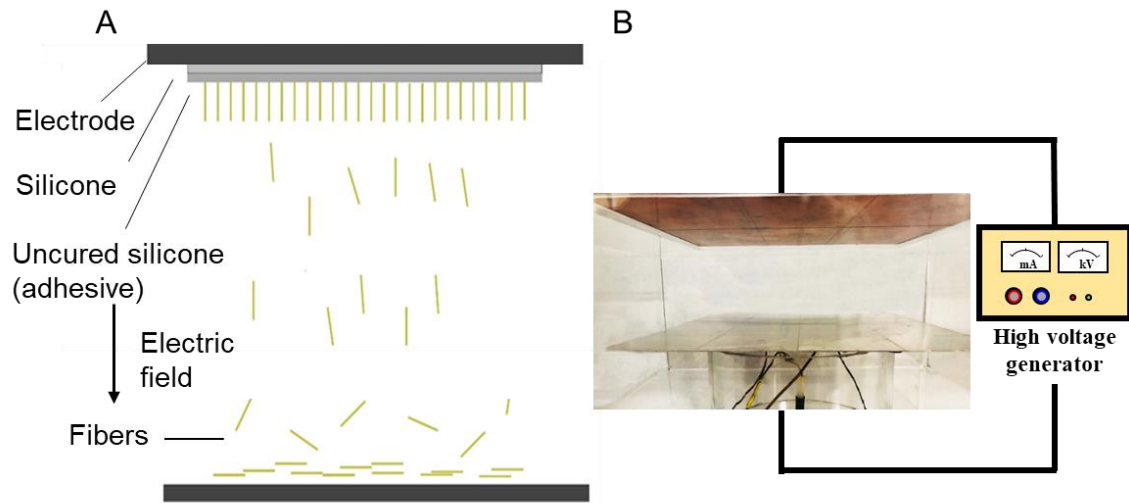


Figure S3. (A)The schematic diagram and (B) the device of electrostatic flocking.

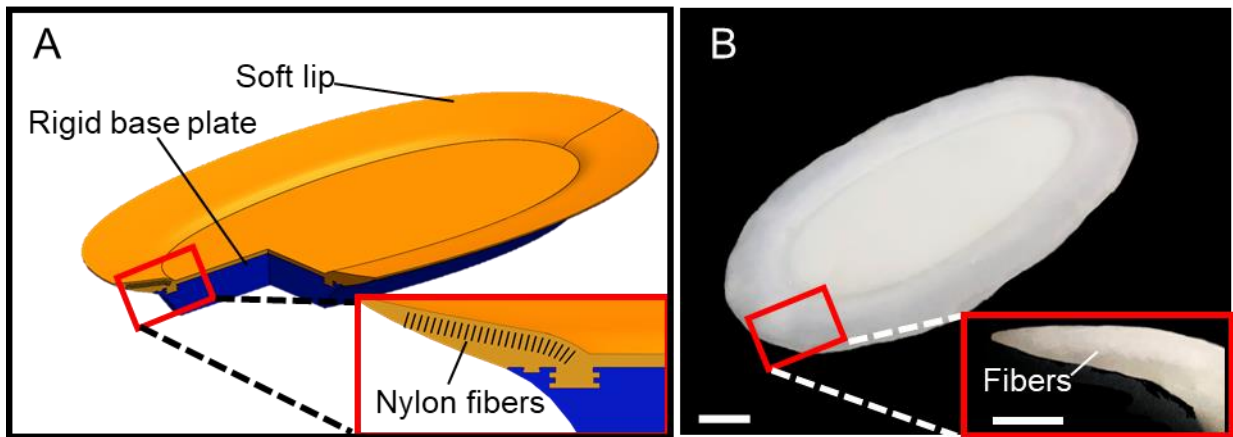


Figure S4. (A) The schematic diagram and (B) the photo image of the biomimetic fiber-reinforced remora disc. Scale bar, 10 mm. The inset in (B) highlights the fibers. Scale bar, 5 mm.

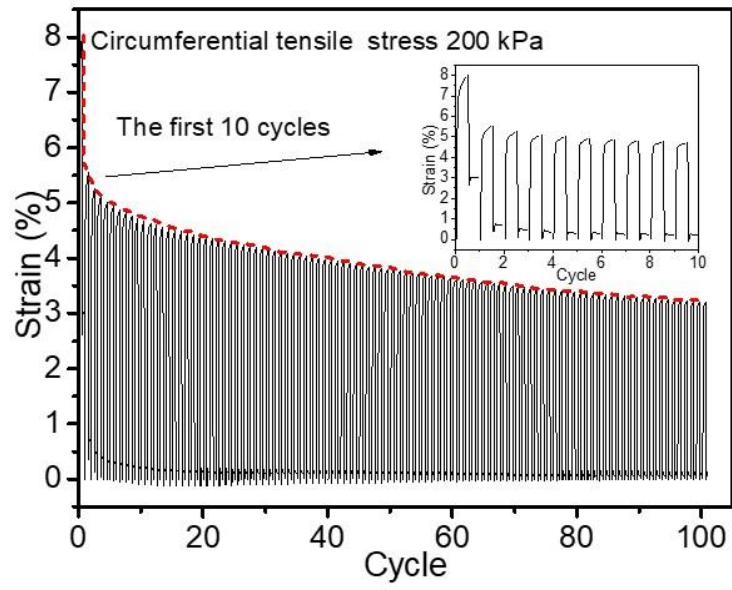


Figure S5. Cyclical creep curve of lip tissue in circumferential tension. When the cyclic creep stress increases to 200 kPa, the creep strain becomes inconsistent through the cycles, confirming the stiffening effect of such stress history.

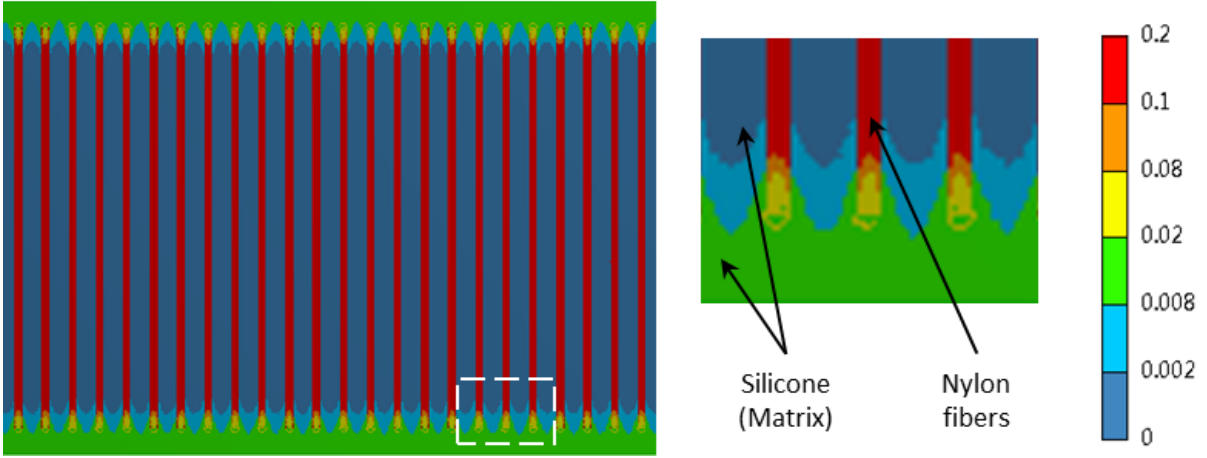


Figure S6. Von-Mises stress distribution of vertical nylon fibers-silicone composite with two layers of silicone at both ends under 10 kPa tensile stress.

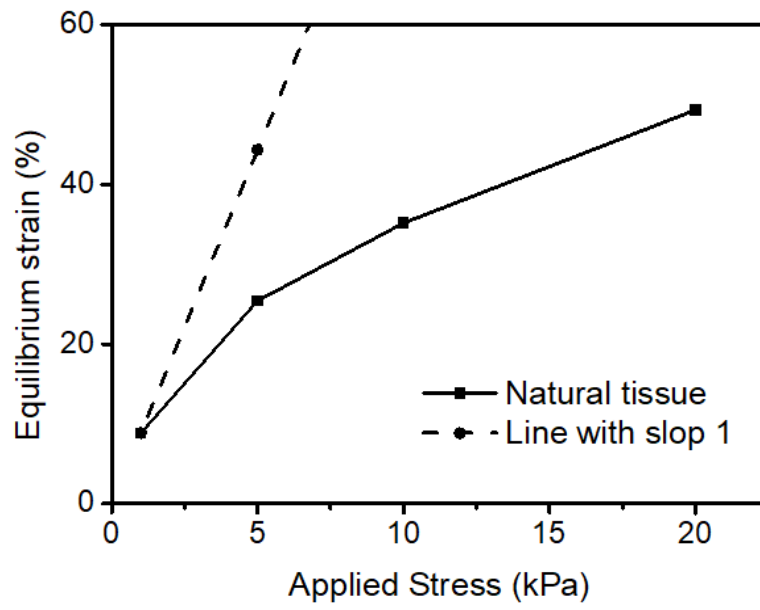


Figure S7. Equilibrium strain as a function of applied stress during the vertical compressive creep experiments in natural lip tissue.

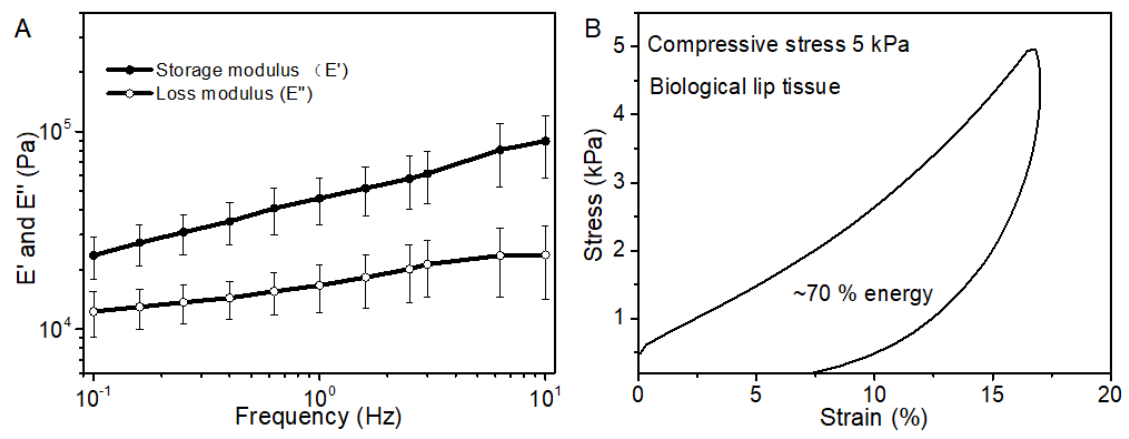


Figure S8. The frequency-sweep curve (A) and loading-unloading test (B) of remora lip tissue in compression (N=5). Error bars, \pm SD.

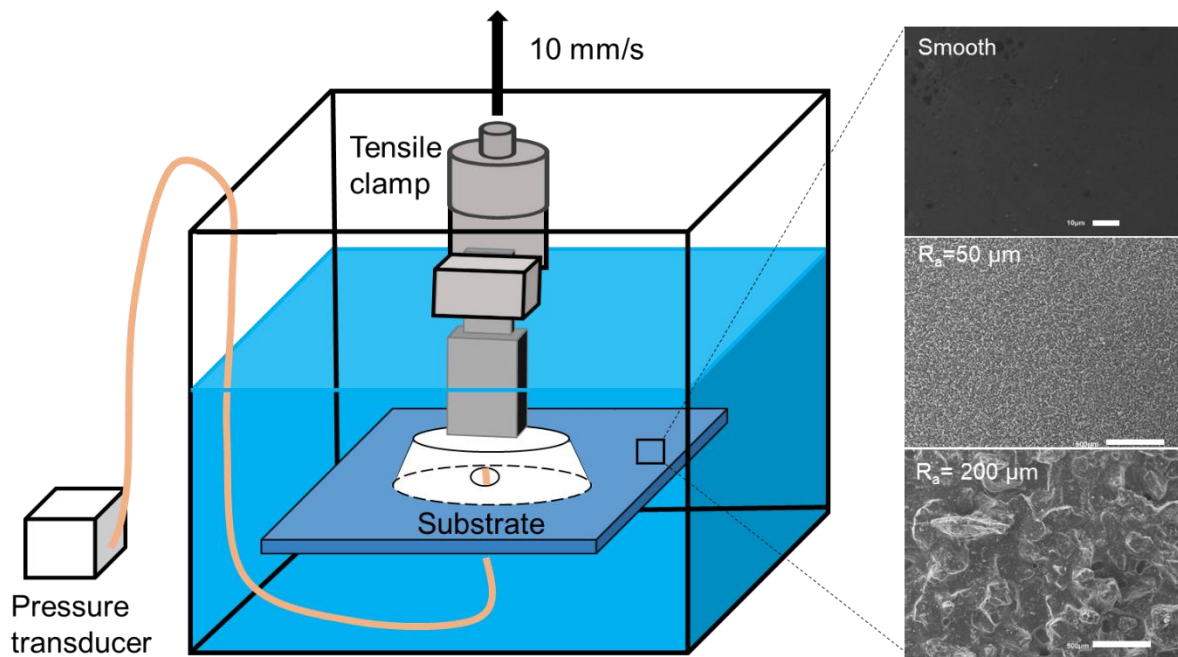


Figure S9. Experimental setup of pull-off forces and pressure measurements on the smooth/rough substrate. Smooth substrate. Scale bar, 10 μm . Rough substrates. Scale bars, 500 μm .

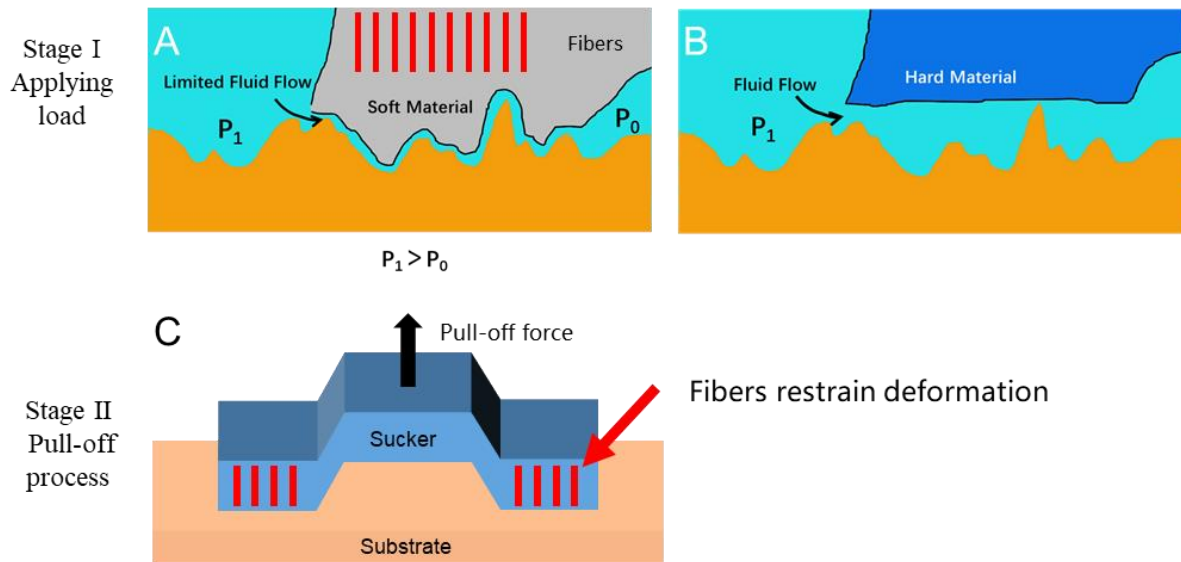


Figure S10. The process of attachment and detachment of biomimetic remora disc underwater. Adhesive disc made of soft material limiting the water flow-in (A), and adhesive disc made of hard material (B), allowing water flow-in. Pull-off process (C), during which higher vertical tensile modulus fibers reduce vertical deformation.

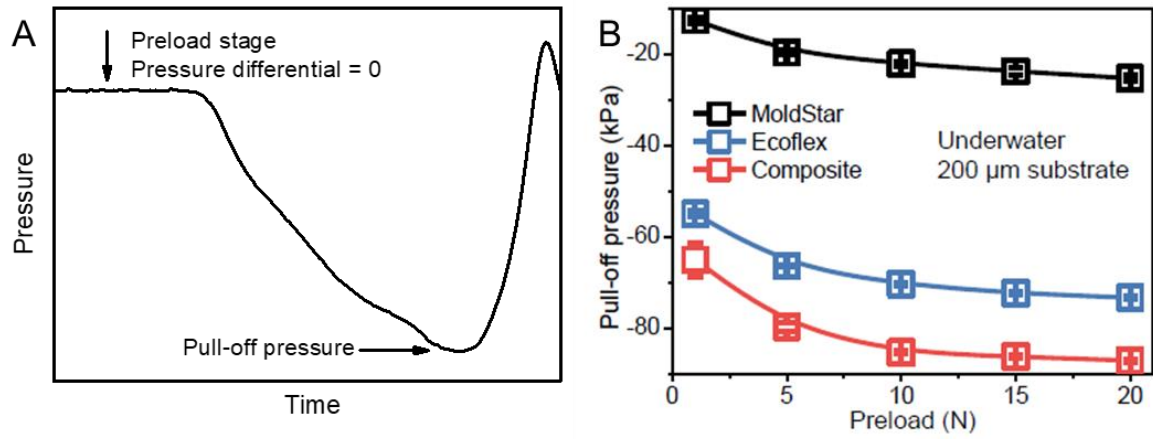


Figure S11. The pressure differential between the inside and outside of the disc chamber increased during the pull-off process (A) and pull-off pressure-preload relationship (B) on a 200- μm surface underwater ($N=5$). Error bars, $\pm\text{SD}$.

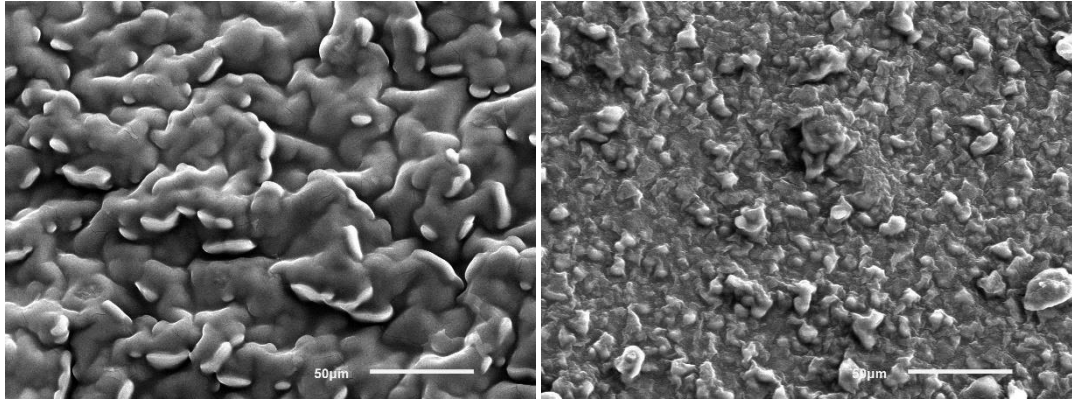


Figure S12. The surface of the Ecoflex (left) is rougher than the surface of MoldStar (right). The magnification of the images is 500 \times . Scale bars, 50 μm .

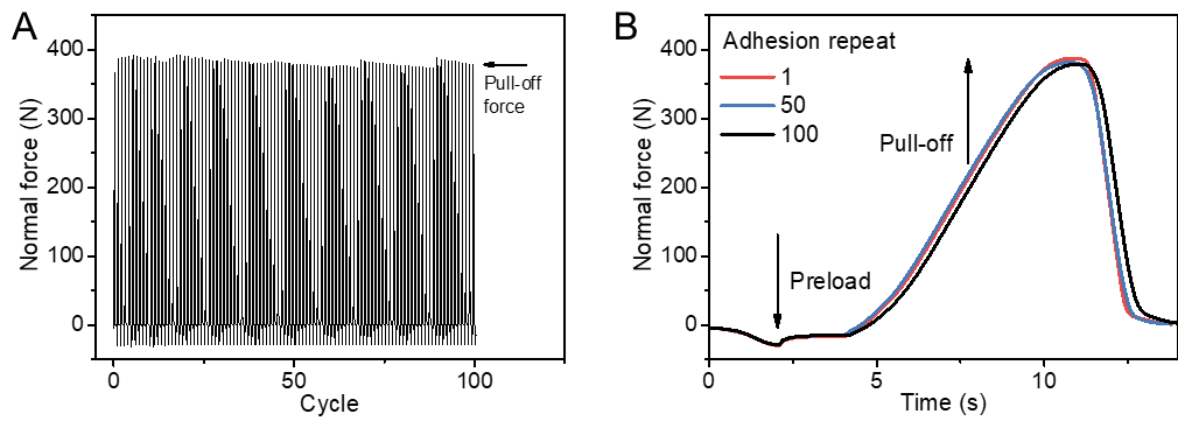


Figure S13. (A) Attachment-detachment cycles: the biomimetic sucker was first subjected to a 15 N preload for 2 s to perform a seal on smooth substrate underwater. (B) The biomimetic sucker could maintain 100 times attachment-detachment cycles without a reduction in pull-off force.

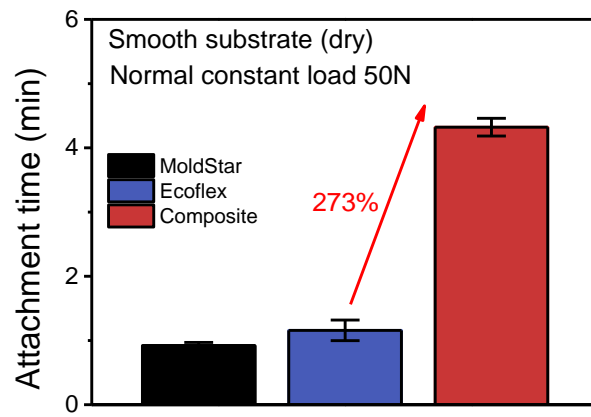


Figure S14. Attachment time of the suckers under 50 N constant load on a dry smooth substrate (N=5). Error bars, \pm SD.

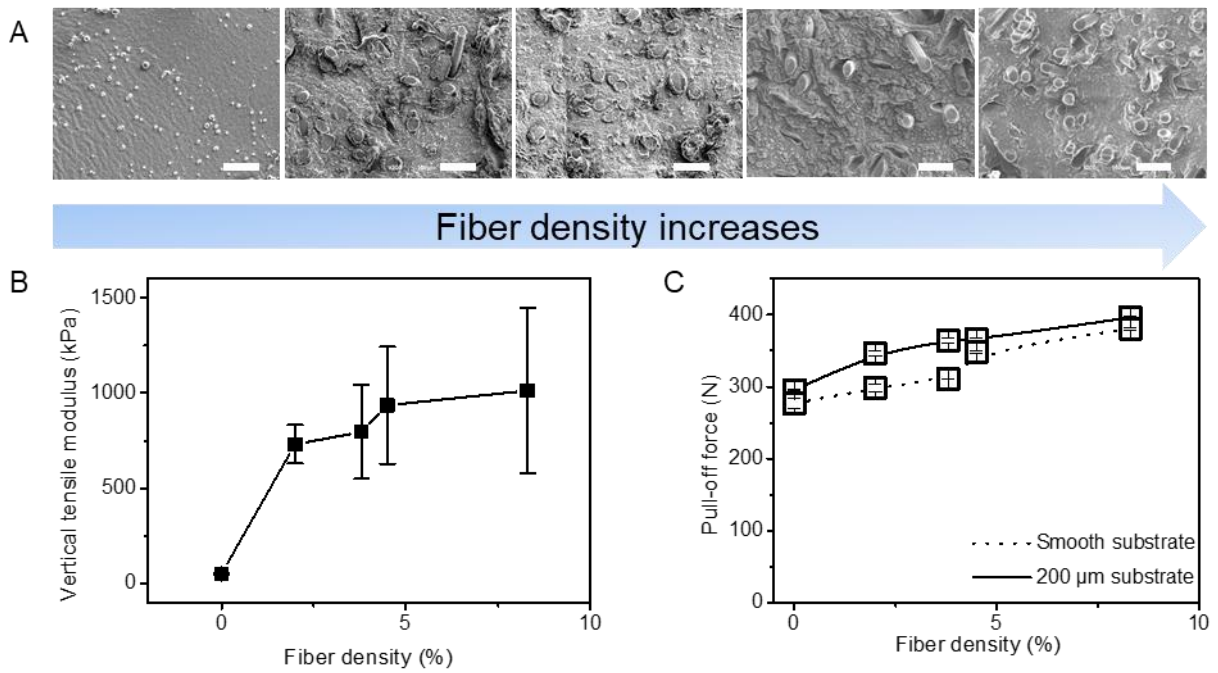


Figure S15. (A) The SEM morphologies of pure silicone and composites with 4 fiber densities. Scale bars, 100 μm . (B) The vertical tensile modulus of silicone or composites and (C) pull-off forces of corresponding suction discs on smooth and rough substrate underwater with preload of 10 N with varied fiber densities ($N=5$). Error bars, $\pm\text{SD}$.

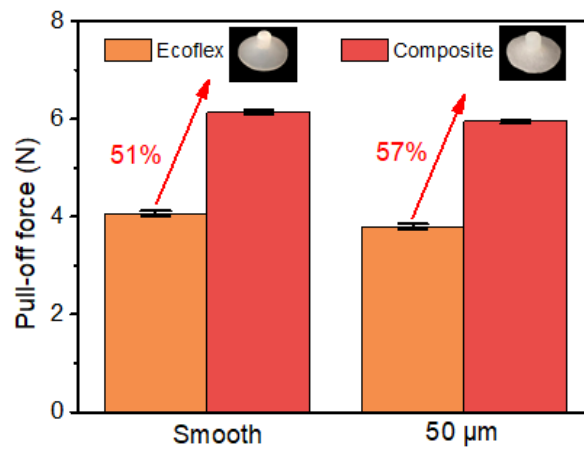


Figure S16. Pull-off forces of common and fiber-reinforced circular suction cups with 0.5 N preload on smooth and rough ($R_a=50 \mu\text{m}$) surfaces underwater (N=5). Error bars, $\pm\text{SD}$.

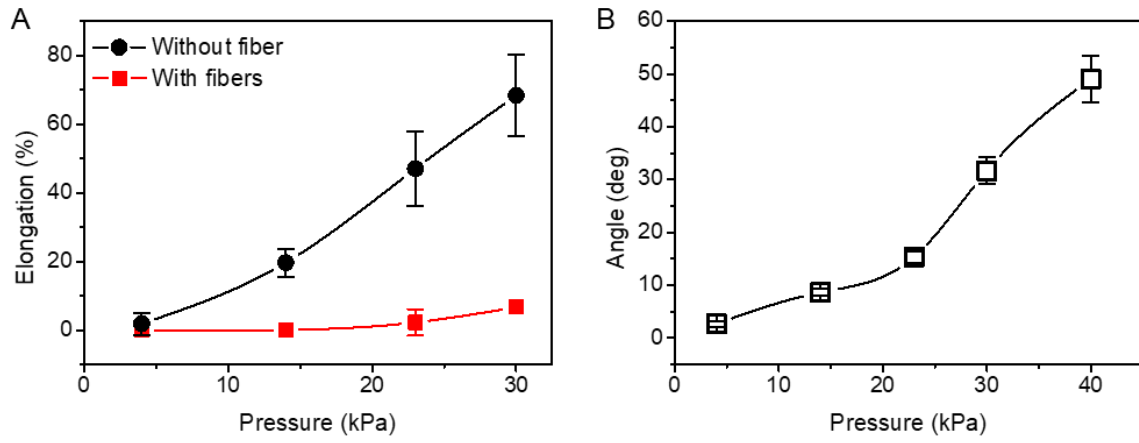


Figure S17. (A) Elongation-pressure curves of actuators with and without fibers. (B) The angle-pressure curve of bending actuator with fibers on one side (N=5). Error bars, \pm SD.

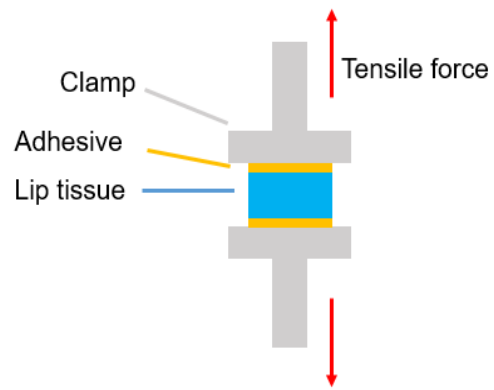


Figure S18. Schematic diagram of vertical tensile modulus testing.

Supplemental Tables

Table S1. Morphological parameters of each remora's adhesive disc.

	Remora 1	Remora 2	Remora 3
Long axis of disc (mm)	72.2	63.3	59.6
Short axis of disc (mm)	26.4	24.7	21.8
Disc aspect ratio	2.7	2.6	2.7
Average disc lip width (mm)	3.4	3.0	2.8
Disc area (mm ²)	1598	1268	1305

Table S2. Physical parameters of the biomimetic remora disc prototype.

Biomimetic remora disc	
Long axis of disc (mm)	130.0
Short axis of disc (mm)	75.0
Disc aspect ratio	1.73
Average disc lip width (mm)	17.0
Disc area (mm ²)	7758

Table S3. Summary of four parameters in the Burgers model for tensile creep behaviors of the rubber, natural tissue and composite.

Parameters	Rubber matrix	Natural tissue	Composite
E_1 (kPa)	55.5±0.3	1415±43	891±25
E_2 (kPa)	321±14	1952±101	2025±1
τ (s)	78±9	62±9	34±5
η (GPa·s)	2.5±0.8	5.8±0.8	5.7±0.7
Adj. R^2	0.97	0.97	0.96

Table S4. Stiffness of the components in the biomimetic prototype.

Materials	Young's Modulus (MPa)
Ecoflex 0020	0.055
Mold Star 30	0.622
Photosensitive resin UTR9000	2589-2695
Nylon fiber	~2000

Supplemental References

1. Militký, J., and Jabbar, A. (2015). Comparative evaluation of fiber treatments on the creep behavior of jute/green epoxy composites. *Compos. B Eng.* *80*, 361-368.
2. Georgiopoulos, P., Kontou, E., and Christopoulos, A. (2015). Short-term creep behavior of a biodegradable polymer reinforced with wood-fibers. *Compos. B Eng.* *80*, 134-144.

Supplemental Experimental Procedures

Experimental Animals

Remoras from Hainan province, China, were used for the investigation. All remoras were euthanized with MS-222. Then the lip tissue was cut off into blocks according to the test requirements. The remoras used in the study were euthanized in accordance with Regulations for the Administration of Affairs Concerning Experimental Animals issued by Institutional Animal Care and Use Committee of Beijing.

Determination of remora lip tissue water content

The wet weight of lip tissues was determined after surface moisture was removed by wiping. Then the lip tissues were treated with 110 °C over 10 min and the dry weight was recorded. The water content was calculated by wet/dry mass.

Finite element analysis

The commercial software ANSYS was employed for the determination of the stress distribution of the suction disc materials under tensile stress. The model (length~2.4 mm, thickness~1.7 mm) contained a composite with an 8% fiber volume fraction and two layers of pure silicone rubber (thickness~0.1 mm) on both sides. Each cylindrical fiber was surrounded by a regular hexahedral silicone model. The tetrahedron elements were adopted. The lower side was fixed and the upper side was applied tensile stress of 10 kPa.

Applicability of creep models for rubber matrix, natural tissue and biomimetic composite

The Burgers model containing a Maxwell and a Kelvin-Voigt element in series is a commonly used model for describing the creep behavior of the polymer and fiber-reinforced composite,^{1,2} in which the creep strain can be represented by the following equation:

$$\varepsilon = \frac{\sigma}{E_1} + \frac{\sigma}{E_2} \left[1 - \exp\left(-\frac{t}{\tau}\right) \right] + \frac{\sigma}{\eta} t \quad (1)$$

where ε is the creep strain, σ is the applied stress, t is the time, E_1 and E_2 are the elastic moduli of the Maxwell and Kelvin model, η is the viscosity of Maxwell model and τ is the retardation time. After applying the tensile stress, the rubber matrix, natural tissue and the composite displayed a sharp elastic strain and a slow viscous and viscoelastic strain development as a function of time. After unloading, the elastic strain instantly recovered and the viscous strain slowly decreased.

Experimental substrates

We created three substrates of different surface roughness (smooth, $R_a=50, 200 \mu\text{m}$). We used molds made from silicone (Dragonskin 20), two different types of sandpapers (FEPA Grit designations P240 and P80, corresponding to average grain sizes of 47 μm and 201 μm , respectively) and glass, and then cast substrates using same epoxy resin system (Araldite LY1564/Aradur3486, Huntsman Corporation, USA). The substrates can not only provide homogeneous surface roughness, but also identical material properties.